MCB
Journals.ASM.org

Ablation of Dihydroceramide Desaturase 1, a Therapeutic Target for the Treatment of Metabolic Diseases, Simultaneously Stimulates Anabolic and Catabolic Signaling

Monowarul M. Siddique,[a] Ying Li,[a] Liping Wang,[b] Jianhong Ching,[a] Mainak Mal,[a] Olga Ilkayeva,[b] Ya Jun Wu,[c] Boon Huat Bay,[c] Scott A. Summers[a,b]

Program in Cardiovascular and Metabolic Disorders, Duke-National University of Singapore Graduate Medical School, Singapore, Singapore[a]; Sarah W. Stedman Nutrition and Metabolism Center, Duke University Medical Center, Durham, North Carolina, USA[b]; Department of Anatomy, National University of Singapore, Singapore, Singapore[c]

The lipotoxicity hypothesis posits that obesity predisposes individuals to metabolic diseases because the oversupply of lipids to tissues not suited for fat storage leads to the accumulation of fat-derived molecules that impair tissue function. Means of combating this have been to stimulate anabolic processes to promote lipid storage or to promote catabolic ones to drive fat degradation. Herein, we demonstrate that ablating dihydroceramide desaturase 1 (Des1), an enzyme that produces ceramides, leads to the simultaneous activation of both anabolic and catabolic signaling pathways. In cells lacking *Des1*, the most common sphingolipids were replaced with dihydro forms lacking the double bond inserted by Des1. These cells exhibited a remarkably strong activation of the antiapoptotic and anabolic signaling pathway regulated by Akt/protein kinase B (PKB), were resistant to apoptosis, and were considerably larger than their wild-type counterparts. Paradoxically, *Des1*$^{-/-}$ cells exhibited high levels of autophagy. Mechanistic studies revealed that this resulted from impaired ATP synthesis due in part to decreased expression and activity of several complexes of the electron transport chain, particularly complex IV, leading to activation of AMP-activated protein kinase and its induction of the autophagosome. Thus, Des1 ablation enhanced starvation responses but dissociated them from the anabolic, prosurvival, and antiautophagic Akt/PKB pathways.

Cells and organisms undergo a series of highly coordinated adaptations to respond to the energy status of their environment. Nutrient abundance upregulates anabolic and prosurvival signaling pathways while inhibiting catabolic and autophagic events that promote nutrient degradation. A central regulator of these responses is the serine/threonine kinase Akt/PKB, which phosphorylates a host of intracellular substrates to promote the storage of simple substrates into complex storage molecules (e.g., glycogen, triglyceride, and protein) and block apoptosis, autophagy, and catabolism (1–3). When external energy stores are scarce, cells and tissues switch into a starvation mode characterized by the induction of autophagosomes and the activation of catabolic enzymes. A key regulator of this starvation adaptation is AMP-activated protein kinase (Ampk), which is activated by rising AMP/ATP ratios (4, 5).

In many obese individuals, adipose tissue expandability and insulin action are compromised, such that the body is incapable of storing nutrients in inert depots and locales. As a result, lipid metabolites like ceramide and diacylglycerol accumulate in peripheral tissues not programmed to store triglycerides in large quantities. In these tissues, such as skeletal muscle, the vascular endothelium, or the liver, they interfere with insulin signaling and action (6–10). As this insulin resistance further impairs nutrient homeostasis, excessive fats are continuously delivered to various peripheral tissues, and the lipotoxic intermediates that accumulate can have disastrous effects on tissue function. For example, disruption of Akt/protein kinase B (PKB) signaling by ceramide renders some cell types, such as pancreatic β cells, susceptible to apoptosis (11, 12).

Two therapeutic strategies have emerged to combat lipotoxicity and insulin resistance. One is to find the means of enhancing the anabolic response to promote the safe storage of nutrients into inert macromolecules. For example, thiazolidinediones, which were once widely prescribed (13), promote adipocyte differentiation and induce enzymes that promote triglyceride synthesis and thus increase the capacity of the organism to safely store fat (14). A second approach has been to promote catabolism of the harmful metabolites. For example, metformin induces mitochondrial dysfunction, leading to a compensatory upregulation in Ampk and an enhanced starvation response, even when fuel is abundant (15). Both of these strategies have proven efficacious and improve insulin sensitivity, but neither fully restores most individuals to health.

More recently, attempts have been made to target specific enzymes that produce lipotoxic molecules such as ceramide. Indeed, inhibitors of enzymes driving ceramide biosynthesis improve insulin sensitivity (16) while preventing diabetes (12, 16), cardiomyopathy (17), atherosclerosis (18), hypertension (10), and hepatic steatosis (19, 20) in rodents. Dihydroceramide desaturase 1 (Des1) inserts an important double bond into the sphingosine backbone of prevalent sphingolipids. The drug fenretinide, which is in clinical trials for the treatment of insulin resistance and cancer (21), inhibits Des1, lowers peripheral ceramide levels, improves insulin sensitivity, and prevents hepatic steatosis in animal

Received 25 February 2013 **Returned for modification** 20 March 2013
Accepted 27 March 2013
Published ahead of print 1 April 2013
Address correspondence to Scott A. Summers, scott.summers@duke-nus.edu.sg.
M.M.S. and Y.L. contributed equally.

doi:10.1128/MCB.00226-13

models (20, 22, 23). Moreover, mice that are haploinsufficient for Des1 are protected from lipid- and glucocorticoid-induced insulin resistance (16) and diet-induced hypertension (10). Thus, the enzyme has emerged as an attractive therapeutic target for treating insulin resistance and associated metabolic diseases.

To gain insight into the molecular mechanisms linking Des1 inhibition to the improvement in insulin action and nutrient metabolism, we evaluated the effects of Des1 ablation on cellular bioenergetics and anabolic/catabolic signaling. As shown herein, embryonic fibroblasts lacking both alleles encoding Des1 demonstrated a marked increase in Akt/PKB signaling, anabolism, and protection from starvation-induced apoptosis. This was anticipated and is likely the result of the depletion of ceramide, an antagonist of Akt/PKB (24). Surprisingly, Des1 ablation also led to the induction of starvation responses, including the activation of Ampk and the induction of autophagy. This was due to dihydroceramide impairment of mitochondrial function, which resulted in decreased ATP synthesis. Thus, Des1 ablation placed cells in a unique state where they underwent a starvation response even under conditions when they were replete with and storing nutrients. Moreover, it disconnected Akt/PKB and its substrate mTOR from autophagic inhibition. These findings suggest important new mechanisms by which ceramide depletion and/or dihydroceramide induction can improve nutrient homeostasis and provide support for the idea that Des1 inhibitors would be beneficial for the treatment of lipotoxicity.

MATERIALS AND METHODS

Cell lines. Mouse embryonic fibroblasts (MEFs) from Des1 wild-type or Des1-null mice generated by Lexicon Pharmaceuticals (The Woodlands, TX) were described previously (16). All cell lines were cultured in Dulbecco's modified Eagle's medium (DMEM) supplemented with 10% fetal calf serum (HyClone; Thermo Scientific) in a water jacket incubator in the presence of 7.5% CO_2 at 37°C.

Western blotting. Cells were lysed in an extraction buffer (66 mM Tris [pH 7.4], 2% SDS) in the presence of a protease inhibitor cocktail (Sigma), incubated on ice for 15 min, and sonicated briefly. The lysate was centrifuged at 10,000 × *g* at 4°C for 30 min, and the supernatant was collected. Protein amounts were quantified using a BCA protein assay kit (Thermo Scientific). Extracts were mixed with loading dye (2% SDS, 10 mM dithiothreitol [DTT], 60 mM Tris [pH 8.0], 1% bromophenol blue, and 15% glycerol) before resolving by SDS-PAGE. After electrophoresis, the separated proteins were transferred by electrotransfer to a polyvinylidene difluoride (PVDF) or nitrocellulose membrane, and loading was checked by staining with Ponceau Red (FLUKA). The membrane was blocked in 1× TTS (10 mM Tris and 0.15 M NaCl, pH 7.6) and 5% nonfat milk for 1 to 2 h at room temperature. After being washed with wash buffer (1× TTS, 0.2% Tween 20, and 0.5% nonfat milk), the blot was incubated with the indicated primary antibody for 2 h at room temperature or 4°C overnight. After 3 washes, the blot was incubated for 1 h with a secondary antibody (anti-mouse or anti-rabbit IgG) conjugated to horseradish peroxidase. Detection was performed using the ECL nonradioactive detection system (Amersham) and an ImageQuant 350 (GE Healthcare). For some antibodies, detection was done using fluorescently labeled secondary antibodies (DyLight, Thermo Scientific) and an Odyssey scanner (LI-COR Inc., Lincoln, NE).

siRNA-mediated knockdown of Ampk. Cells were transfected with siRNA specific for Ampk [Ampkα1 siRNA(m), SC-29674; Santa Cruz Biotechnology] using Lipofectamine RNA interference (RNAi) MAX (Invitrogen, Life Technologies Corporation) according to the manufacturer's protocol. Cells were trypsinized and split into 10-cm tissue culture dishes 24 h before transfection in order to have them approximately 70% confluent at the time of the experiment. The culture medium was replaced with Opti-MEM (Invitrogen) containing 20 nM of small interfering RNA (siRNA) mixed with 1 ml of Opti-MEM reduced-serum medium and 35 μl of Stealth RNAi-Lipofectamine 2000. These were mixed gently and incubated at room temperature for another 15 min before being added to the cells. After 3 h of incubation, serum was added. Fourteen to 16 h later, the Lipofectamine-containing culture medium was removed, and the cells were washed with PBS and grown in normal serum-containing medium. Experiments were conducted 48 h later.

Analysis of lipids. (i) Sample preparation. To quantify levels of specific lipids, cells were harvested, washed with ice-cold phosphate-buffered saline (PBS), and spiked with an internal standard mixture (C_{17}-sphingosine, C_{17}-sphinganine, C_{17}-sphingosine 1-phosphate, C_{17}-sphinganine 1-phosphate, C_{12}-ceramide, C_{12}-ceramide 1-phosphate, C_{12}-glucosylceramide,C_{12}-lactosylceramide, C_{12}-sphingomyelin, and 14:0 phosphocholine from Avanti Polar Lipids). Thereafter, the cells were resuspended in 900 μl of ice-cold chloroform-methanol (1:2) and incubated in ice for 15 min with vortexing every 5 min. Three hundred microliters of ice-cold distilled water (dH_2O) and 300 μl of ice-cold chloroform were added to the samples, which were then vortexed and centrifuged at 8,000 × *g* for 2 min at 4°C. The lower organic phase was transferred into a clean microcentrifuge tube. A second extraction was performed by adding 300 μl of ice-cold chloroform, and the lower organic phase was pooled with that of the first extraction. The collected samples were dried under a stream of nitrogen and stored at −80°C until ready for liquid chromatography tandem mass spectrometry (LC-MS/MS) analysis.

(ii) Lipidomic profiling. The dried samples were reconstituted in 1:1 chloroform-methanol and analyzed by an LC system (Agilent 1260 Infinity) coupled with electrospray MS/MS (Agilent 6430 triple quadruple MS). A Zorbax Hilic Plus column (2.1-mm internal diameter by 50 mm; 1.8-μm particle size) from Agilent was used. For the LC method, a flow of 0.4 ml/min was used. Mobile phase A consisted of acetonitrile-water (95:5); mobile phase B consisted of acetonitrile-water (50:50); both mobile phases contained 10 mM ammonium acetate and were adjusted to pH 8.0. For the analysis, 2 μl of sample was injected. Analysis was performed by increasing the mobile phase A/B ratio from 100:0 to 50:50 in 10 min and then to 20:80 in 0.5 min. The A/B ratio was returned to 100:0 in 0.5 min and held linearly for another 5 min. Nitrogen was used as the nebulizing gas, and the flow was set at 6 liters/min. The capillary was set at 4,000 V, and the gas temperature was set at 300°C.

Dihydrosphingomyelin was analyzed by monitoring the masses of the parent together with a transition of *m/z* 184, which corresponds to a loss of the P-choline head group. In this case, particular species will not be able to be differentiated from sphingomyelin species with similar carbon chain lengths [i.e., this method will not be able to distinguish between SM(d18:1/18:0), SM(d18:0/18:1), and SM(16:1/20:0)]. In the case for ceramide and its corresponding dihydroceramide, such a problem does not exist. Ceramides and dihydroceramides were monitored by the mass of the parent together with a transition of *m/z* 264 and *m/z* 266, respectively. The transition of *m/z* 264 and *m/z* 266 corresponds to the loss of sphingosine and sphinganine, respectively. For glucosylated ceramides, a HILIC column was used for separation. Glucosylceramide and lactosylceramide were analyzed, and their retention times were around 0.6 min and 1.9 min, respectively.

Immunofluorescence. MEFs were cultured on coverslips and serum deprived for the indicated period of time. They were then fixed in 4% paraformaldehyde at room temperature for 30 min. After being washed with PBS, cells were permeabilized in 0.2% Triton for 20 min at room temperature. After several washes, cells were blocked in 10% goat serum for 30 min at room temperature. Primary antibodies were diluted in 10% goat serum and incubated with the slide for 2 h at room temperature or overnight at 4°C. Samples were washed again and incubated with a fluorescently labeled secondary antibody for 1 h at room temperature. Coverslips were then mounted on slides using Vectashield mounting medium containing DAPI (4′,6-diamidino-2-phenylindole). The slides were stored at −20°C and analyzed using a Carl Zeiss confocal microscope.

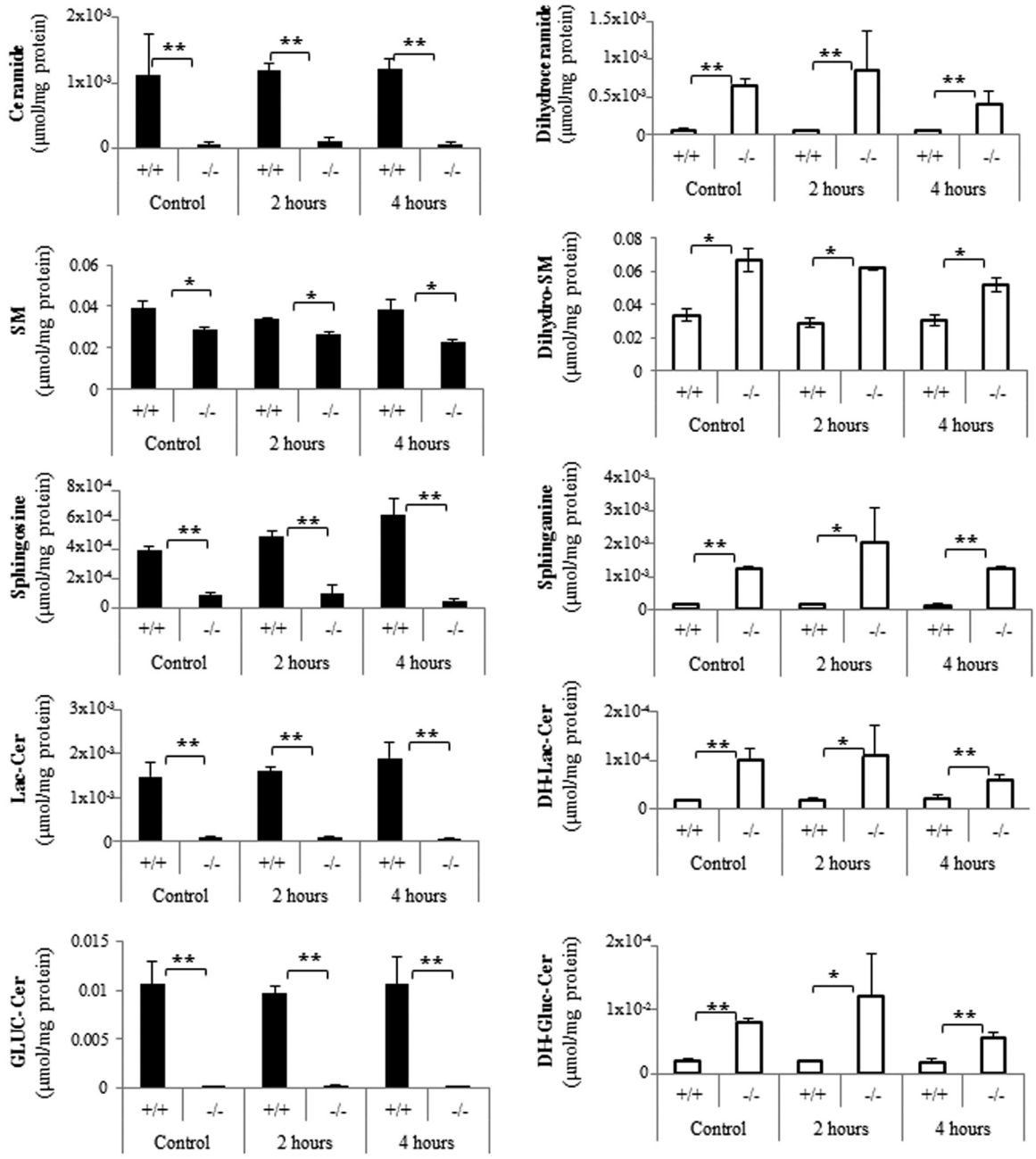

FIG 1 Sphingolipid profiles in Des1$^{+/+}$ and Des1$^{-/-}$ MEFs. Wild-type and knockout MEFs were subjected to serum deprivation for 0 (control), 2, or 4 h. Lipids were extracted as described, and sphingolipid levels were detected by LC-MS/MS. SM denotes sphingomyelin, Lac denotes lactosyl, DH denotes dihydro, Gluc denotes glucosyl, and Cer denotes ceramide. **, $P < 0.01$; *, $P < 0.05$; $n = 3$.

Mitochondrial staining. MitoTracker Green FM (Invitrogen) was used to stain mitochondria according to the manufacturer's instructions. Briefly, the MitoTracker reagent was diluted in DMEM (100 nM) and added to the culture. After 30 min of incubation at 37°C, the cells were washed 3 times with DMEM and mounted on slides by using warm culture medium. Slides were analyzed immediately with a confocal microscope.

Measuring mitochondrial oxygen consumption. Cells were seeded in XF24 cell culture plates (5,000/well) with 100 μl of growth medium and incubated at room temperature for 1 h. A total of 150 μl of growth medium was added, and the cells were incubated in a tissue culture incubator overnight. Cells were washed once with prewarmed XF assay medium and incubated in 500 μl of 1× assay medium (XF assay medium; Seahorse Bioscience, Chicopee, MA) for 1 h at 37°C in the absence of CO^2. Rotenone (1 μM) plus antimycin A (1 μM), oligomycin (1 μM), and carbonylcyanide-4-(trifluoromethoxy)-phenylhydrazone (FCCP) (0.3 μM) were added to prevent electron transfer by various mitochondrial electron transfer chain components during the measurement of O_2 consumption using the XF24 analyzer (Seahorse Bioscience, Chicopee, MA).

Measurement of mitochondrial respiration chain function. Cells were harvested with trypsin, and a million cells/ml were assayed in 2 ml MiR05 medium (0.5 mM EGTA, 3 mM $MgCl_2$, 60 mM K-lactobionate, 20

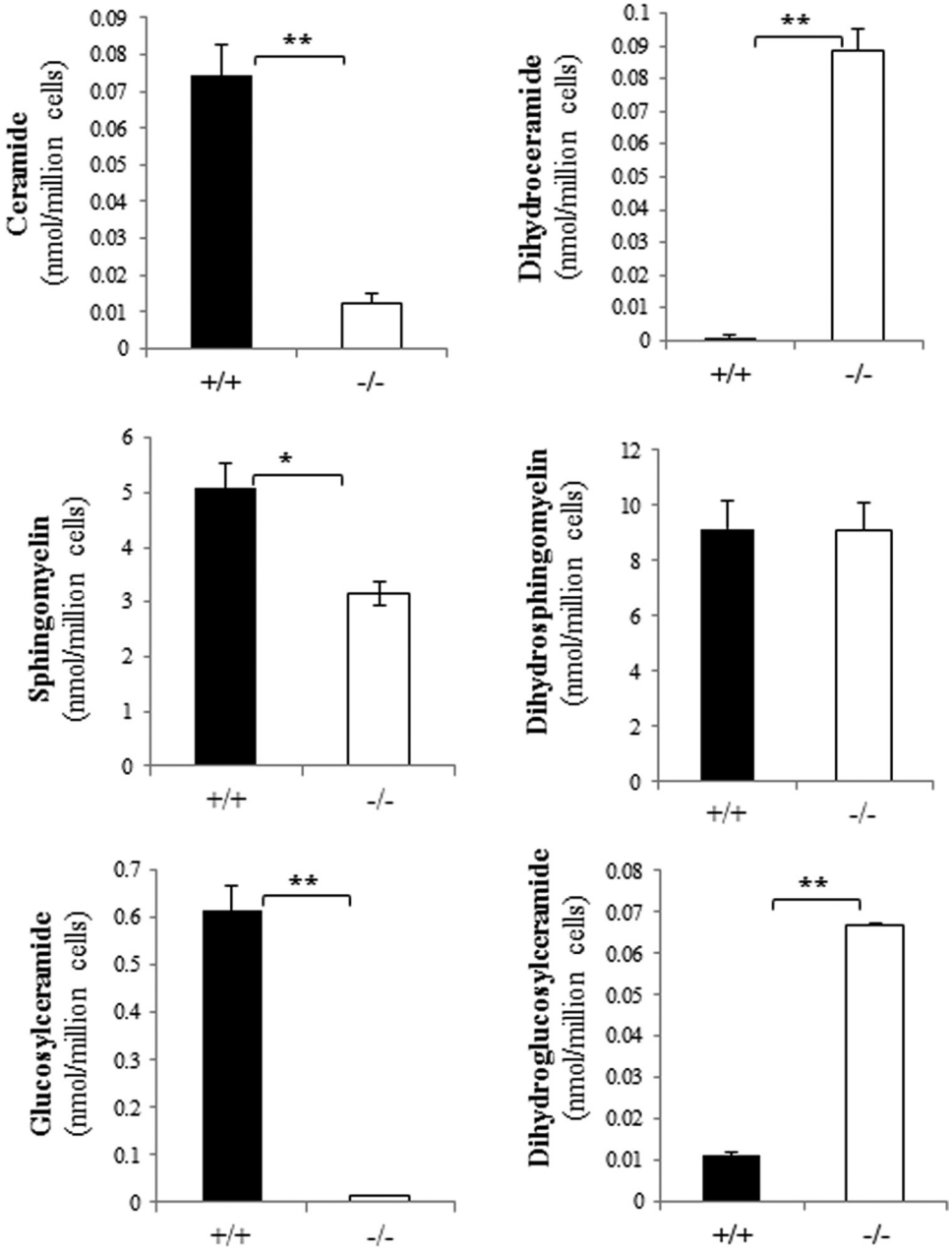

FIG 2 Des1 ablation alters the sphingolipid content of isolated mitochondria. Mitochondria were isolated as described previously (61). Lipid levels were quantified by LC-MS/MS as described in Materials and Methods. **, $P < 0.01$; *, $P < 0.05$; $n = 3$.

mM taurine, 10 mM KH2PO4, 20 mM HEPES, 110 mM sucrose, 1 g/liter bovine serum albumin [BSA; essentially fatty acid free]) using the OROBOROS Oxygraph-2k respirometer. Respiratory oxygen flux was measured in real time and expressed as picomoles of O_2 per second per gram of protein. Cells were permeabilized by digitonin. A total of 5 mM pyruvate plus 2 mM malate and 1 mM ADP were added to stimulate complex I respiration. A total of 1 μM rotenone and 5 mM succinate were added to test complex II respiration. A total of 2 mM ascorbate and 0.5 mM *N*,*N*,*N*,*N*-tetramethyl-*p*-phenylenediamine (TMPD) were used to test complex IV respiration.

Measuring ATP levels in cells. Five million cells were pelleted and resuspended in 1 ml ice-cold buffer containing 150 mM KCl, 25 mM Tris-HCl (pH 7.6), 2 mM EDTA (pH 7.4), 10 mM KPO 4 (pH 7.4), 0.1 mM $MgCl_2$, and 50 μg/ml digitonin for 3 min. BSA was added to stop the reaction, and cells were pelleted and resuspended in the same buffer without digitonin but with 2 mM malate and 5 mM pyruvate. ATP synthesis was initiated by the addition of ADP (12.5 μl of 100 mM ATP stock) to a final concentration of 5 mM. Cells were incubated at 37°C for 0 min, 5 min, and 10 min. Aliquots (50 μl) of this reaction mixture were used at each time point for measuring luminescence. The amount of ATP was measured by luminometer (Infinite M200 PRO; TECAN, Switzerland) using the ATP bioluminescence assay kit (FLASC; Sigma-Aldrich) by following the manufacturer's instructions. An aliquot of cell suspension was used for quantifying protein.

Electron microscopy. Cells were seeded onto a coverslip and, after 24 h of culture, fixed with 2.5% glutaraldehyde and washed 3 times with PBS.

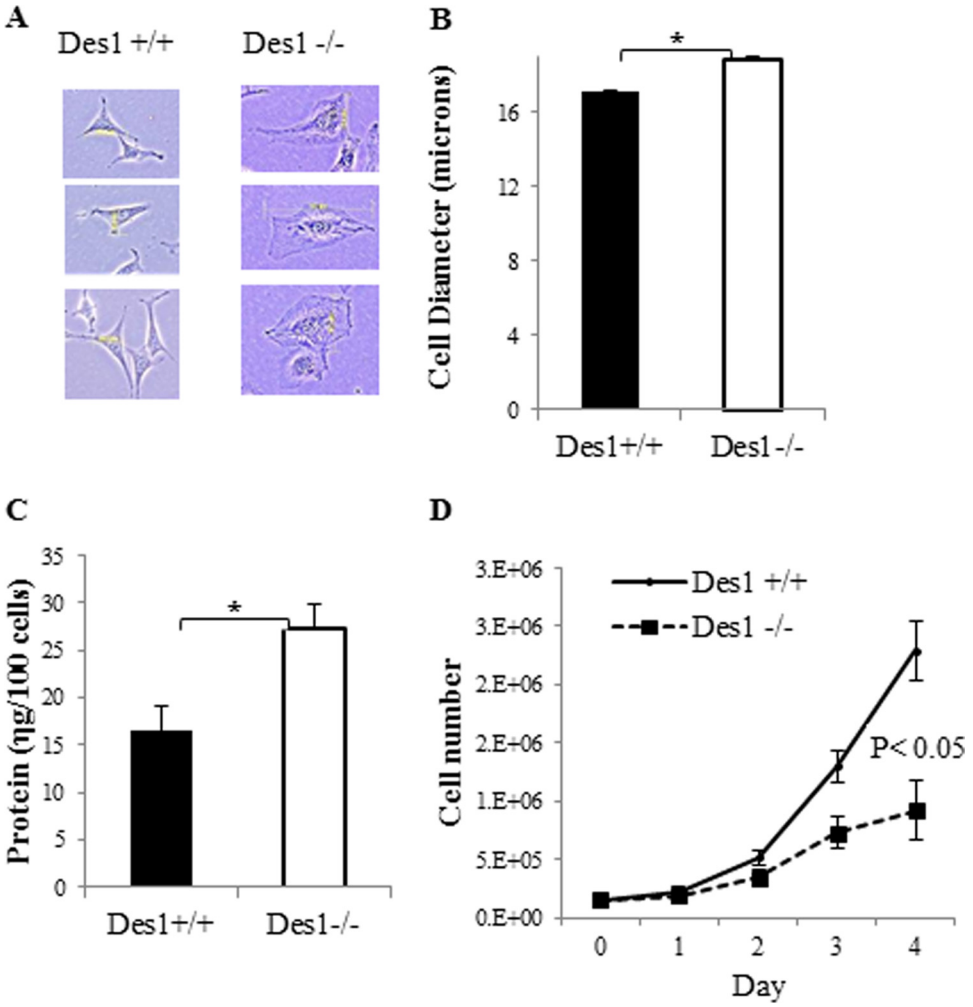

FIG 3 Des1$^{-/-}$ are considerably larger than Des1$^{+/+}$ cells. (A) Representative pictures of Des1$^{+/+}$ and Des1$^{-/-}$ cells obtained from bright-field microscopy. (B) Cell diameter was determined using a Beckman cell counter (2.5×10^5 cells; $n = 3$). (C) Protein levels were determined by BCA in samples normalized for equal cell numbers. (D) Equal numbers of cells were seeded (1.5×10^5) in different plates at day 0 in medium containing 10% FBS. Cell proliferation was assessed by measuring cell number daily using a Beckman cell counter. *, $P < 0.05$; $n = 3$.

The cells were treated with 1% osmium tetroxide followed by dehydration with an ascending series of alcohol before being embedded in araldite. Ultrathin sections were stained with uranylacetate and lead citrate. Images were acquired using the Olympus EM208S transmission electron microscope at the NUHS Electron Microscopy Unit, Singapore.

RESULTS

Des1 ablation markedly alters the sphingolipid profile of cells, generating a host of sphingolipids that lack the double bond present in the ceramide backbone. To quantify levels of common sphingolipids and their dihydro counterparts, lipidomic analysis was performed by the Duke-NUS Metabolomics Facility. As the following studies were often done after serum withdrawal, extracts were also analyzed under comparable experimental conditions. As shown in Fig. 1, Des1 ablation nearly eliminated ceramide, sphingosine, lactosylceramide, and glucosylceramide from the cells. In contrast, the dihydro counterparts of these sphingolipids (i.e., dihydroceramide, sphinganine, dihydrolactosylceramide, dihydroglucosylceramide), which are nearly absent from wild-type cells, accumulated significantly in the knockout strains. Sphingomyelin levels were significantly diminished in the knockout strains, and dihydrosphingomyelin was elevated, but neither of these effects was as dramatic as seen for the other lipids. Dihydrosphingomyelin levels were considerably higher than anticipated in both lines. Starvation didn't have an appreciable effect on sphingolipid levels. Sphingolipids in isolated mitochondria reflected those in the whole cells (Fig. 2).

Des1 ablation altered cell morphology and proliferation. When analyzing the Des1$^{-/-}$ cells under bright field microscopy, one immediately notices that they are considerably larger than Des1$^{+/+}$ cells (Fig. 3A). Cells from the knockout animals had an increased diameter (Fig. 3B) and larger amounts of cellular protein than the wild type (Fig. 3C). Proliferation rates were significantly reduced in the Des1$^{-/-}$ cells (Fig. 3D).

Des1 ablation promoted signaling through Akt/PKB. The marked increase in cell size reminded us of studies in *Drosophila*, where constitutive activation of Akt/PKB leads to an autonomous increase in cell size (25). Moreover, ceramides have long been known to inhibit Akt/PKB (24, 26), and one might predict that

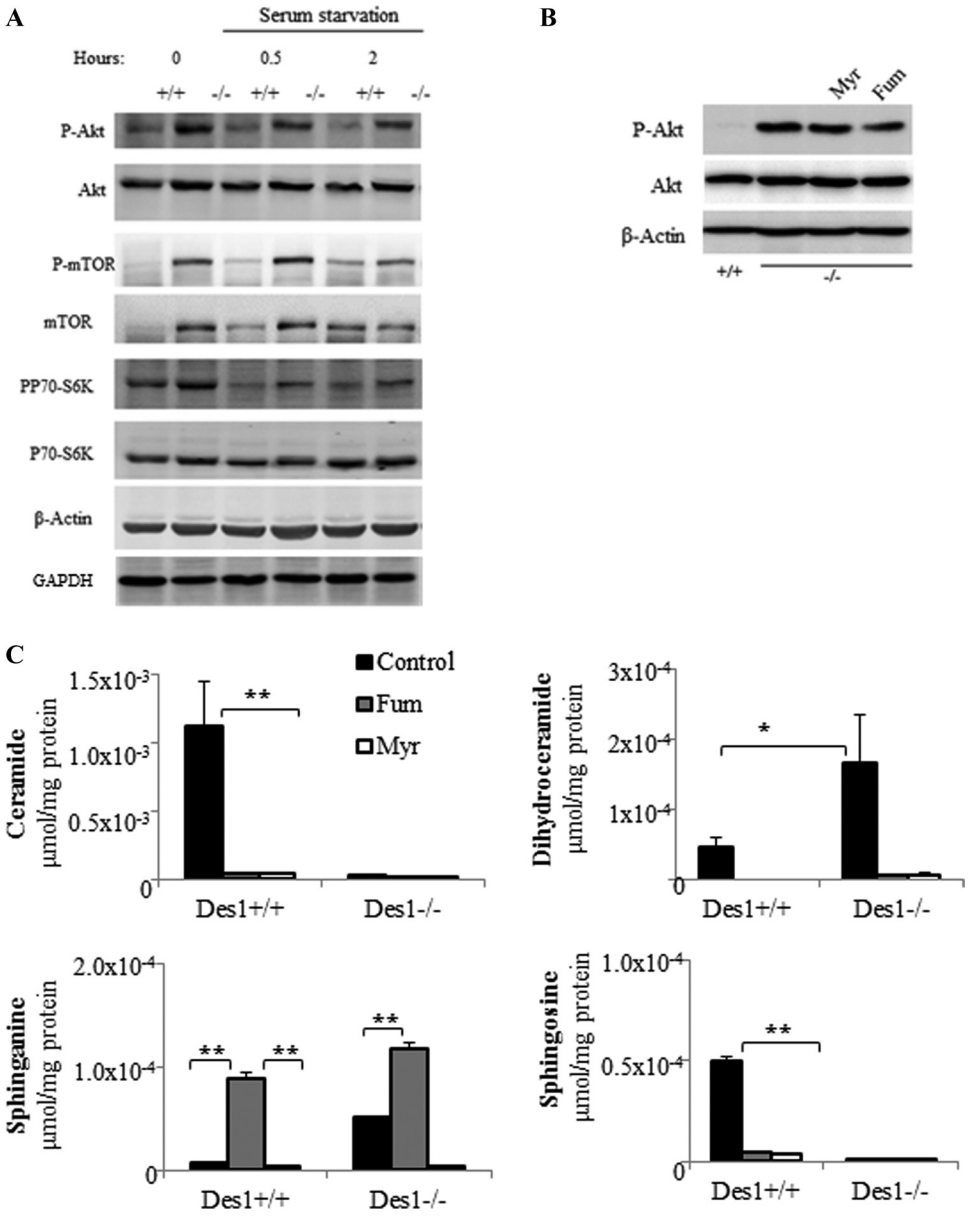

FIG 4 Des1 ablation activates the Akt/mTOR signaling pathway. (A) Wild-type and knockout cells were serum deprived for 0 (control), 30 min, or 2 h. Lysates were obtained and resolved by SDS-PAGE before immunoblotting with the indicated antibodies. (B) Cells kept in normal serum were treated with either vehicle (DMSO), myriocin (Myr; 10 μM), or fumonisin B1 (Fum; 50 μM) for 48 h. Data are representative of 3 to 5 independent experiments. *, $P < 0.05$; **, $P < 0.01$; $n = 3$. (C) Fumonisin and myriocin prevent the accumulation of many dihydrosphingolipid species in the Des1$^{-/-}$ cells. Cells were treated with fumonisin (50 μM) or myriocin (10 μM) for 48 h before lipid extraction. Sphingolipid levels are quantified by LC-MS/MS as described in Materials and Methods. **, $P < 0.01$; *, $P < 0.05$; $n = 3$.

their absence would lead to increased Akt/PKB phosphorylation and activity. As predicted, Des1 ablation resulted in constitutive Akt/PKB phosphorylation (Fig. 4A). Moreover, kinases downstream of Akt/PKB that facilitate its anabolic responses (e.g., mTOR, pp70 S6-kinase) were also constitutively phosphorylated (Fig. 4A).

A question emerging from these studies is whether it is the (i) absence of ceramide-derived sphingolipids or (ii) the presence of dihydroceramide-based sphingolipids that accounts for the effect on Akt/PKB. Prior studies have revealed that short-chain analogs of ceramide, but not dihydroceramide, inactivate Akt/PKB, suggesting that ceramide is the dominant regulator. However, we have found that short-chain dihydroceramide is not appreciably absorbed in cells, nor is it metabolized effectively through the salvage pathway to generate other sphingolipids. While others have reported biological effects for dihydroceramides, we feel its exogenous use is fraught with problems and that the model herein is superior for testing the effects of endogenous sphingolipids. To test whether endogenous dihydroceramides are key regulators of Akt/PKB, we treated cells with two different inhibitors of enzymes upstream of Des1 in the sphingolipid *de novo* synthesis pathway. Myriocin, which inhibits serine palmitoyltransferase, and fumo-

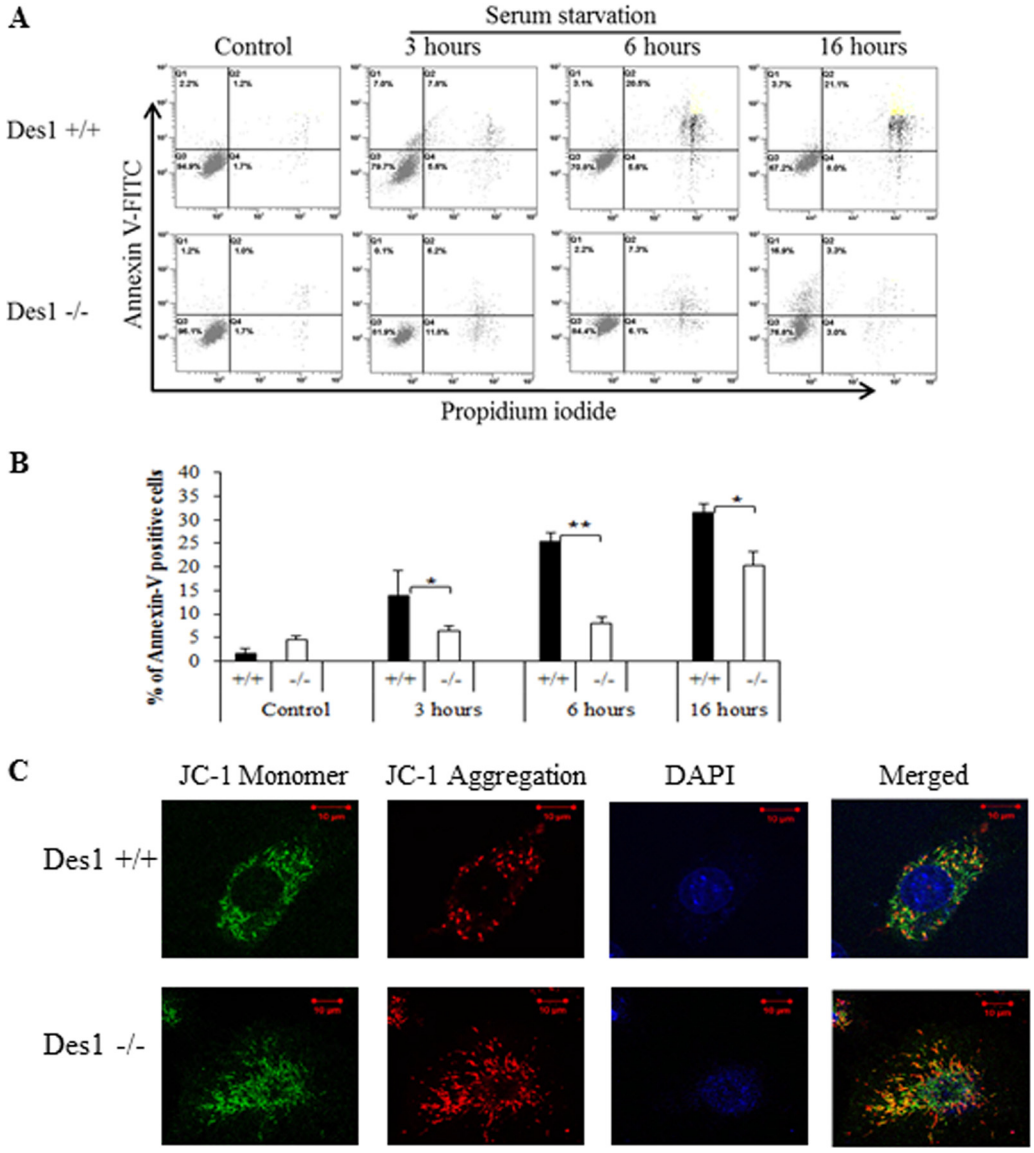

FIG 5 Des1 ablation renders cells resistant to apoptosis induced by serum withdrawal. (A) Wild-type and knockout cells were analyzed by staining for annexin V (*y* axis [FL1]; apoptotic cells) or propidium iodide (*x* axis [FL3]; dead cells) at either 0 (control), 3, 6, or 16 h after serum withdrawal. Cells stained with the indicated reagent were quantified by FACS analysis. (B) Quantification of cells undergoing late apoptosis as assessed for panel A, above. *, $P < 0.05$; **, $P < 0.01$; $n = 3$. (C) JC-1 staining of $Des1^{+/+}$ and $Des1^{-/-}$ indicates higher mitochondrial membrane potential in $Des1^{-/-}$ cells. Green fluorescence on the left represents monomeric JC-1 in the cytoplasm, while red fluorescence represents J-1 aggregates accumulated in mitochondria due to high mitochondrial membrane potential.

nisin B1, which inhibits (dihydro)ceramide synthases, did not markedly reduce Akt phosphorylation (Fig. 4B), but they completely eliminated ceramide, sphingosine, and dihydroceramide from the cells (Fig. 4C). Thus, endogenously generated ceramides are the likely antagonists of Akt/PKB phosphorylation, and dihydroceramides are unlikely to be stimulators.

Des1 ablation protects cells from apoptosis caused by serum withdrawal. In addition to regulating protein synthesis through mTOR and pp70 S6-kinase, Akt/PKB is an antiapoptotic factor (27–29). Moreover, ceramide has long been identified as a potential inducer of apoptosis caused by serum deprivation (30, 31) and other stress stimuli (32, 33). Thus, one would predict that Des1 ablation might protect cells from apoptosis and cell death caused by serum withdrawal. This hypothesis proved correct as determined by fluorescence-activated cell sorting (FACS) analysis using annexin V-fluorescein isothiocyanate (FITC) and propidium iodide (PI) staining (Fig. 5A and B). Moreover, staining with JC-1 revealed that the $Des1^{-/-}$ cells had higher mitochondrial membrane potential (Fig. 5C), revealing that the membranes were less permeable to protons (34). Thus, Des1 ablation strongly protected cells from apoptosis caused by serum withdrawal.

Des1 ablation induces autophagy. The Merrill group made the interesting discovery that both fenretinide, which inhibits Des1, and exogenous, short-chain dihydroceramides induce autophagy (35, 36). However, Akt/PKB and mTOR are well established antiautophagic molecules. Therefore, we were curious

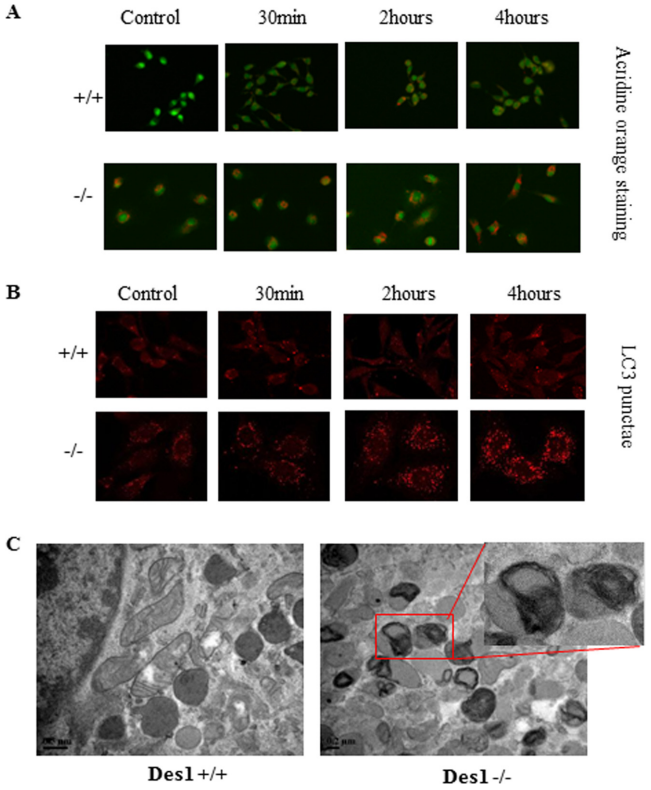

FIG 6 Des1 ablation increases autophagy in MEFs. (A) Cell serum deprived for the indicated period of time before staining with acridine orange to visualize autophagic vesicles. (B) Cells were serum deprived as described for panel A before staining with LC3 to visualize punctae indicative of autophagic vesicles. (C) Cells were assessed by electron microscopy to visualize various organelles. As highlighted by the red box, numerous multimembrane structures were present in the knockout cells, suggesting an increase in basal autophagy.

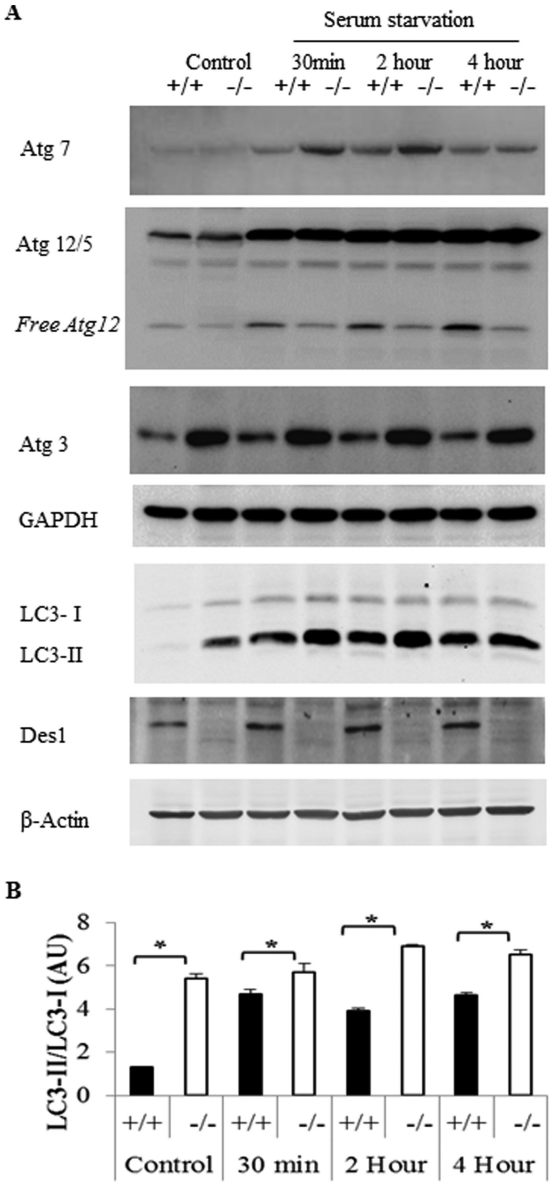

FIG 7 Des1 ablation increases expression of a number of autophagy proteins. (A) Knockout and wild-type cells were serum deprived as indicated, and cell lysates were resolved by SDS-PAGE and immunoblotted with antibodies recognizing Atg7, Atg12, Atg3, LC3, and Des1. Data are representative of 3 independent experiments. (B) Quantitative analysis of LC3-II/LC3-I ratios under the conditions described above. *, $P < 0.05$; $n = 3$.

whether the cells described herein, which accumulate dihydroceramides but show a simultaneous activation of Akt/PKB and mTOR, would be (i) prone to or (ii) protected from autophagy. Molecular analysis confirmed that the knockout cells had an elevated level of basal autophagy that was potentiated by serum withdrawal. As shown in Fig. 5, staining acidic autophagic vesicles with acridine orange revealed that the Des1$^{-/-}$ cells had a large increase in such organelles (Fig. 6A). Moreover, antibodies against the microtubule-associated protein 1 light chain 3 II (LC3-II), a well-recognized marker for autophagosomes, confirmed this finding. LC3 containing punctate foci were not detectable in control cells and were sparsely distributed after 2 and 4 h of starvation. However, LC3 containing punctae were detectable in the Des1$^{-/-}$ cells under both normal and serum-deprived conditions (Fig. 6B). Transmission electron microscopy images confirmed that large numbers of autophagic vesicles accumulated in the Des1$^{-/-}$ cells (Fig. 6C).

LC3 is posttranslationally modified by a ubiquitin-like system to form LC3-I and LC3-II, the latter being the membrane-bound form that is associated with autophagic vesicles (37). LC3-II degrades when the autophagosome fuses with lysosomes or endosomes, and its disappearance reflects the completion of an autophagic event. To prevent the disappearance of the processed LC3-II during autophagy, we added the protease inhibitors E64 (cysteine protease inhibitor) and pepstatin A (inhibitor of acid proteases) to the culture at the time of serum withdrawal. This allowed for detection of both forms of LC3 (LC3-I and LC3-II) by Western blotting. LC3-II levels were consistently higher in Des1$^{-/-}$ cells than Des1$^{+/+}$ cells in untreated conditions, as well as following serum deprivation (Fig. 7).

Other markers of autophagy were also altered in the knockout cells. Atg7, an E1-like enzyme involved in the initiation of the autophagic response, was elevated 30 and 120 min after serum starvation (Fig. 7). The Atg5/12 complex forms because of a covalent interaction driven by Atg7 that is required for the formation of the autophagosome. Atg 5/12 levels were induced by starvation

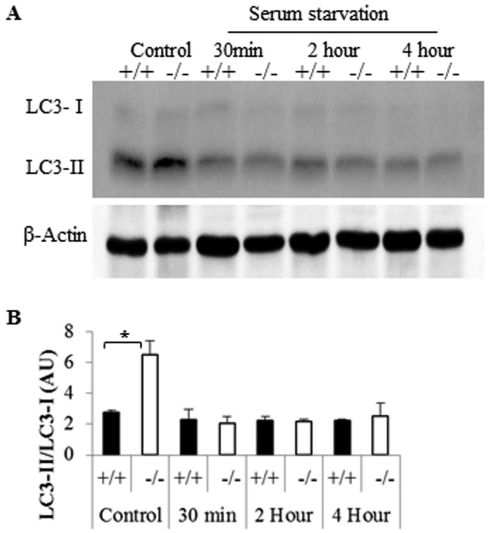

FIG 8 Des1 ablation does not block autophagic flux. (A) Cell lysates were treated as described for Fig. 7 except pepstatin and E64 protease inhibitors were not added to the lysing medium. (B) Quantitative analysis of LC3-II/LC3-I ratios. *, $P < 0.05$; $n = 3$.

in both cell lines, despite the fact that free Atg12 levels decreased in the Des1$^{-/-}$ cells. A portion of Atg3, an E2-like protease, binds to Atg12 during autophagy. Atg12/3 conjugation requires Atg7 for the activation of Atg12. Strikingly higher levels of Atg3 were detected in the Des1$^{-/-}$ cells (Fig. 7). Collectively, these observations suggest that basal autophagic processes are upregulated in the Des1$^{-/-}$ cells, and the process accelerates following nutrient deprivation.

LC3-II can accumulate due to either an increase in the number of autophagic events or because of a diminution of the rate of autophagic flux and thus LC3-II degradation. To rule out the latter, we detected LC3-II without adding protease inhibitors following serum starvation. LC3-II quickly disappeared under such conditions, indicating that the rate of LC3-II was not affected by Des1 depletion (Fig. 8). Instead, the data support the hypothesis that the elevated levels of LC3-II result from an increase in the number of autophagic vesicles being formed.

Des1 ablation-induced autophagy is Ampk dependent. The dissociation between Akt/mTOR and autophagy was surprising, since mTOR is deemed to be a dominant regulator of the cellular process. These data suggest that these knockout cells sense starvation conditions, even at a time when anabolic signaling through Akt/PKB is elevated and they are replete with nutrients. We sought to determine the molecular events responsible for initiating autophagy in the knockout cells. Falling ATP/AMP ratios activate Ampk, and the enzyme is known to stimulate formation of the autophagosome by phosphorylating and activating Ulk1 (38). Specifically, Ampk phosphorylates Ser317 and Ser717 on Ulk1 to drive autophagic events. Under nutrient sufficiency, high mTOR activity typically prevents Ulk1 activation by phosphorylating it on Ser757 and disrupting the interaction between Ulk1 and Ampk (39). However, in the Des1$^{-/-}$ cells, where Akt/PKB and mTOR are activated, the Ampk pathway was dominant. In the knockout cells, Ampk and its target on Ulk1 were phosphorylated more than in wild-type cells in both basal and serum-deprived conditions (Fig. 9A and B). The direct involvement of Ampk in autophagy induction was confirmed using siRNA-mediated Ampk knockdown, which markedly reduced the autophagic processes (Fig. 10).

Ampk activation and autophagy result from mitochondrial impairment that decreases ATP synthesis. As described above, Ampk is a sensor of cellular energy levels. Thus, the Des1 knockout cells are in a unique metabolic state where they are simultaneously showing an induction of anabolic (i.e., Akt/PKB phosphorylation and activation, protein synthesis, and increased survival) and starvation (i.e., Ampk phosphorylation, and autophagy) re-

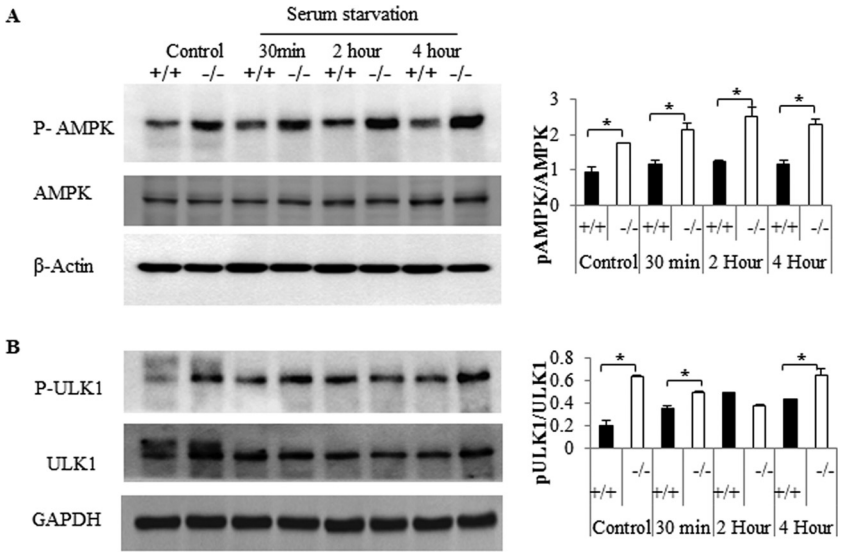

FIG 9 Des1 ablation activates the AMPK/ULK1 pathway. Wild-type and knockout cells were subjected to serum withdrawal for the indicated period of time before being lysed and immunoblotted with antibodies recognizing phospho-AMPK^{Thr172} and AMPK (A) and phospho-ULK1^{Ser555} and ULK1 (B). Ratios of the phosphorylated versus nonphosphorylated forms were quantified, and the data, in arbitrary units, are depicted. Phospho-AMPK and phospho-ULK1 level are elevated in Des1$^{-/-}$ cells at both basal level and after serum starvation, compared to their wild-type counterparts. *, $P < 0.05$; $n = 3$.

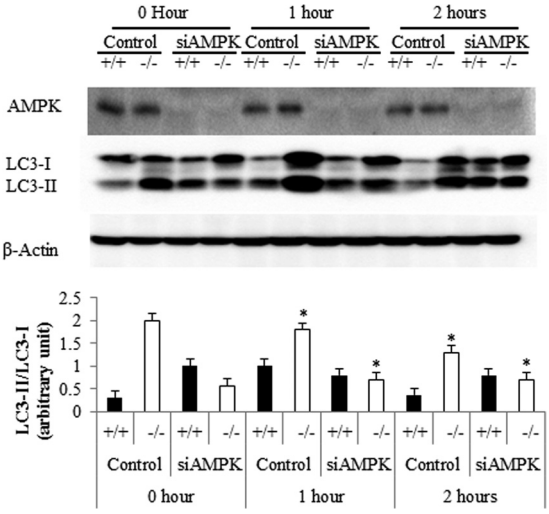

FIG 10 Ampk is an obligate intermediate linking Des1 ablation to the induction of autophagy. Cells were transfected with siRNA targeting AMPK 48 h prior to assessing LC3-II levels. A graph showing LC3-II/LC3-1 ratios is depicted at the bottom. $n = 3$; $P < 0.05$.

sponses. We thus sought to evaluate whether the cells were compromised in their ability to generate ATP. Such mitochondrial dysfunction is the underlying mechanism by which the antidiabetic drug metformin stimulates Ampk to promote lipid oxidation and to subsequently increase insulin sensitivity. Using pyruvate and malate as the substrates, we observed that rates of ATP production were significantly lower in Des1$^{-/-}$ cells than that in wild-type cells (Fig. 11A). When dihydroceramide accumulation was inhibited by myriocin or fumonisin B1 in these cells, initial rates of ATP production returned to wild-type values, suggesting that it was the increase in dihydroceramide that impaired ATP production (Fig. 11B). Thus, unlike Akt phosphorylation, which was due mainly because of the absence of ceramides, the impairment in ATP synthesis is due to the accumulation of dihydroceramide-containing sphingolipids.

To determine the mechanism underlying the impaired ATP synthesis, we characterized mitochondrial respiration in the knockout versus wild-type cells. The numbers of mitochondria, as assessed by MitoTracker, appeared to be comparable in the two cell types (Fig. 12A). Moreover, citrate synthase activity was comparable (Fig. 12B). Using an XF24 extracellular flux analyzer (Seahorse Bioscience), we examined the oxygen consumption rate (OCR). As shown in Fig. 12C and D, the OCR for basal respiration and respiration capacity (induced by adding FCCP) was significantly lower in the Des1$^{-/-}$ cells than in the wild-type cells. Coupled respiration, calculated by subtracting the OCR following treatment with the complex V (ATP synthase) inhibitor oligomycin from the basal OCR, was also lower in the Des1$^{-/-}$ cells. We next evaluated the expression pattern of the various complexes in the electron transport chain. Interestingly, the Des1$^{-/-}$ cells had far less cytochrome *c* oxidase (complex IV) and possibly less complex I and III (Fig. 13A) than wild-type cells. Direct measurement of complex activity confirmed that there was a significant reduction in the activity of complex I and IV (Fig. 13B).

We also used electron microscopy to investigate mitochondrial morphology. We found numerous elongated mitochondria with distorted cristae structures in the Des1$^{-/-}$ cells (Fig. 13C). Many of the mitochondria were unchanged, however, and it is difficult to ascertain whether a change in mitochondrial structure underlies the disappearance of complex IV. As we described above,

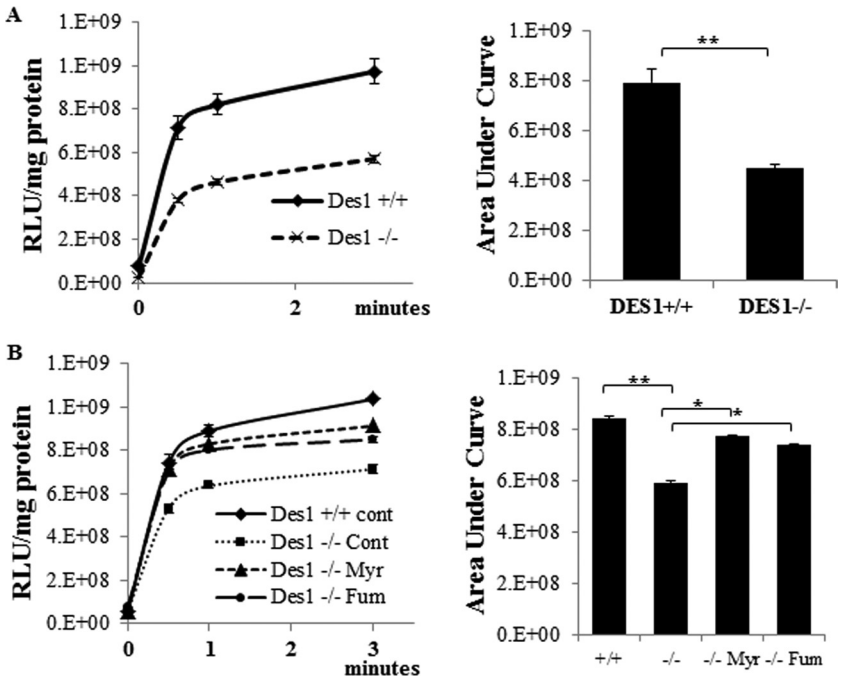

FIG 11 Dihydroceramide impairs ATP production. (A) ATP production was measured in cells permeabilized with digitonin (50 μg per 1 million cells) using pyruvate (5 mM) and malate (2 mM) as the substrates. Shown are the increases in ATP levels following substrate addition. (B) To some cells, myriocin (Myr; 10 μM) or fumonisin (Fum; 50 μM) were added 48 h prior to measuring ATP in order to block dihydroceramide accumulation. (**, $P < 0.05$; $n = 3$).

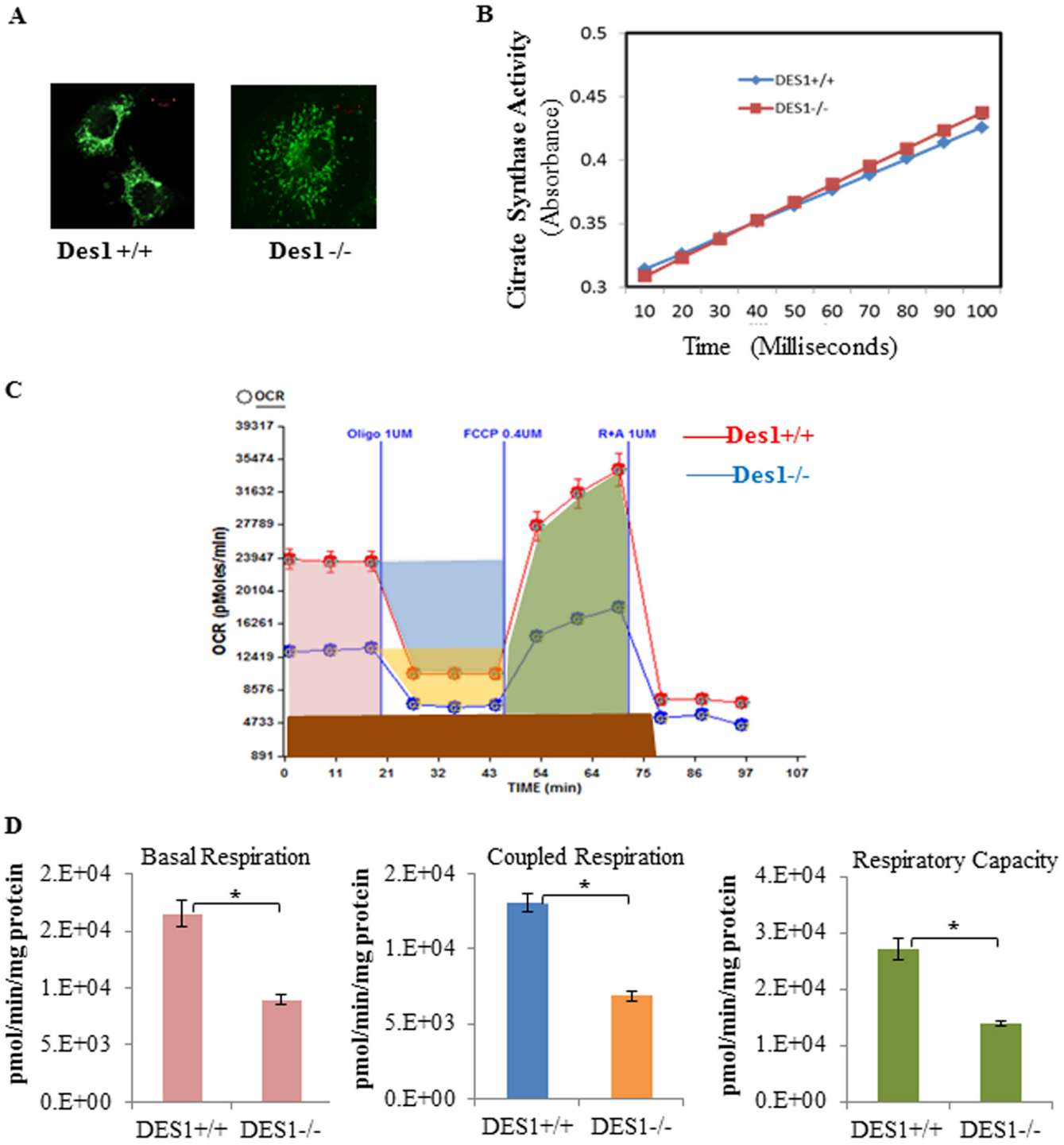

FIG 12 Des1 ablation decreases mitochondrial respiration. (A) Wild-type and knockout cells were stained with MitoTracker to identify the number of mitochondria/cell. (B) Des1 ablation does not alter citrate synthase activity. Citrate synthase activity was determined using the citric acid synthase assay kit (Sigma, MO). Whole-cell lysates were used for citrate synthase activity test. Oxaloacetate was added at time zero. $n = 4$. (C) Oxygen consumption rates (OCR) of $Des1^{+/+}$ and $Des^{-/-}$ cells were measured by a Seahorse XF24 extracellular flux analyzer. OCRs of $Des1^{+/+}$ and $Des1^{-/-}$ are shown in red and blue, respectively. Following a period of measurement to reveal basal respiration, oligomycin was added to measure uncoupled respiration. The subsequent addition of FCCP allowed for the quantification of respiratory capacity, and the addition or rotenone and antimycin A, which block both complex I and II, allowed for determination of residual respiration. (D) Quantitative analysis illustrates the individual determinations obtained for panel A. The represented colors are in accordance with the color labeling in panel A. Residual respiration was deducted from each parameter before calculation; coupled respiration was calculated by deducting uncoupled respiration from basal level respiration. *, $P < 0.05$; $n = 8$.

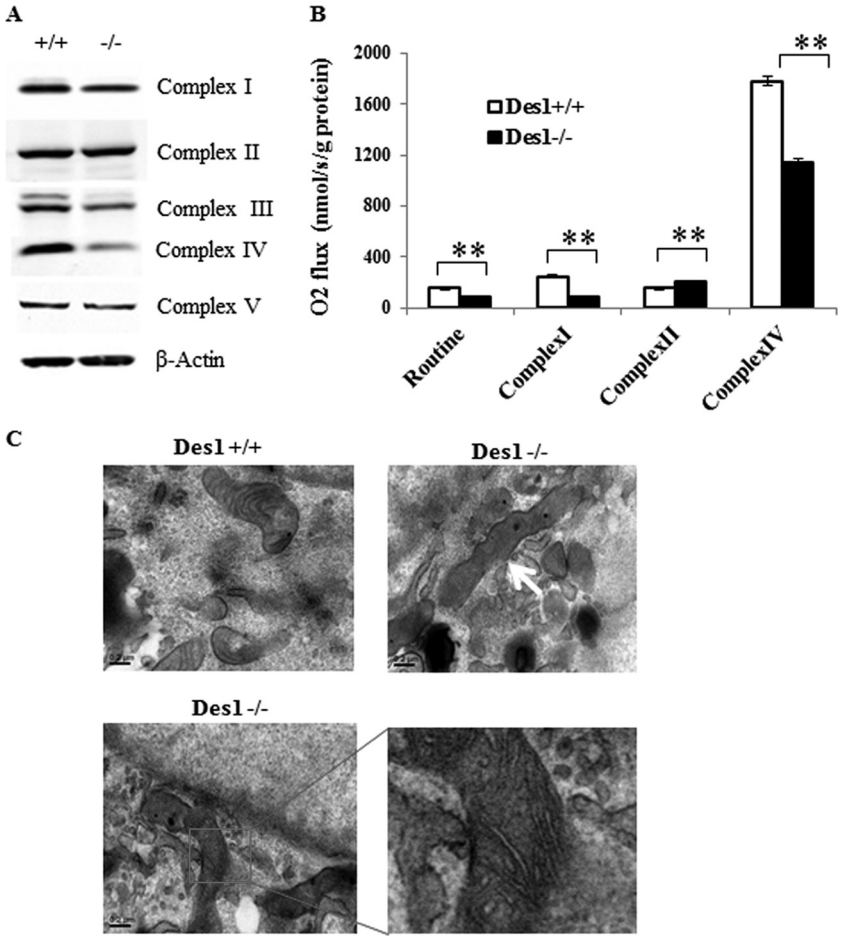

FIG 13 Des1 ablation reduces cytochrome *c* oxidase IV expression and activity. (A) A subunit of each of the respiratory chain complexes was quantified in wild-type (+/+) and knockout (−/−) cells. (B) The activity of complexes I, II, and IV were determined as described in Materials and Methods. **, $P < 0.01$. (C) Electron microscopic images of the cells were obtained. The upper panels show images from wild-type (left) and knockout (right) cells viewed at 40,000× magnification. The occasional elongated mitochondria that we observed are highlighted by the arrow. The bottom panels show an amplified image of the elongated mitochondria with distorted cristae.

mitochondrial membrane potential was actually increased in the knockout cells (34).

The addition of exogenous ATP to Des1$^{-/-}$ cells prevented autophagy upon serum withdrawal. The observations thus far suggest that impairments in ATP synthesis resulting from dihydrosphingolipid accumulation cause cells to undergo starvation responses. To confirm this, we investigated whether the addition of synthetic ATP to Des1$^{-/-}$ cells would prevent autophagic induction. Such treatments have been shown to elevate intracellular ATP levels (40). As shown in Fig. 14, exogenous ATP decreased intracellular levels of LC3-II. These results strongly support the hypothesis that compromised mitochondrial function, resulting in lower ATP production, accounts for the induction of autophagy in the Des1$^{-/-}$ cells.

Amino acids and organic acid levels were unchanged in these cells. Amino acids can inhibit autophagy (41, 42), in part through their ability to allosterically activate mTOR. Metabolomic profiling by the Sarah Stedman Metabolomics Facility at Duke University revealed that amino acid levels were unchanged in the cells and thus were unlikely to be involved in the autophagy upregulation in the knockout cells (Fig. 15). Cellular metabolism, investigated by detecting various organic acids created during anaerobic respiration and the citric acid cycle, was also similar between the two cell lines (Fig. 16). The activity of citrate synthase, a component of the citric acid cycle, was also unchanged (Fig. 12B).

DISCUSSION

In 2007, we demonstrated that decreasing ceramide levels with inhibitors of serine palmitoyltransferase or ceramide synthases ameliorated many features of obesity, including insulin resistance and diabetes. We attributed this to the fact that these compounds reduced levels of ceramide, a known antagonist of the anabolic enzyme Akt. In a more recent study, we investigated the efficacy of Des1 inhibitors and found that they similarly lowered ceramide levels and ameliorated glucose intolerance and insulin resistance, as well as resolving hepatic steatosis. Unlike the inhibitors used earlier, blocking Des1 leads to the accumulation of dihydrosphingolipids, which have recently been identified as potentially bioactive molecules. To gain further insight into the mechanisms by which Des1 inhibition and/or dihydroceramides might alter cell function, we chose to investigate the metabolic consequences of complete Des1 ablation. As predicted, eliminating Des1 led to a

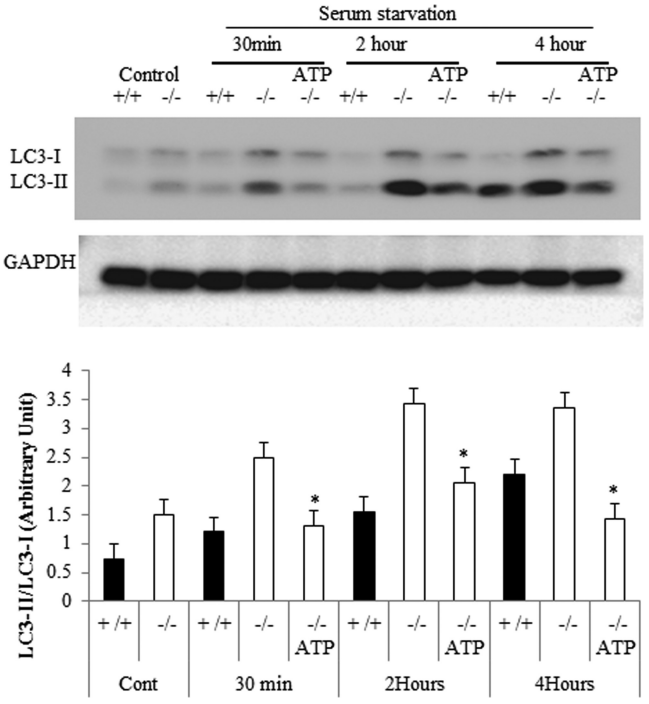

FIG 14 Addition of ATP prevents autophagy caused by Des1 ablation. To determine whether the impairment in ATP synthesis was essential for the induction of autophagy, we supplemented the serum deprivation medium with exogenous ATP (250 μM) and determined LC3-II/LC3-I ratios as described above.

marked upregulation of Akt, an increase in cell survival, and anabolism. Surprisingly, however, ablation of the gene also mimicked actions of the insulin-sensitizing drug metformin by disrupting oxidative phosphorylation and ATP synthesis, thus activating Ampk and promoting catabolic responses (e.g., autophagy). Thus, Des1 depletion places cells in a unique metabolic state where dihydroceramides are driving a starvation response, which is uncoupled from the anabolic pathway regulated by Akt and mTOR (depicted schematically in Fig. 17). These data suggest that Des1 may be an exciting therapeutic target for the treatment of diseases associated with obesity.

Dihydroceramides have received considerable attention in the last few years, owing to an unexpected discovery by the Merrill laboratory that the chemotherapeutic agent fenretinide, previously thought to be an inducer of ceramide synthesis, was actually an inhibitor of dihydroceramide desaturase. Merrill's group conducted lipidomic studies using mass spectroscopy to characterize lipid profiles of cells treated with fenretinide, which had been thought to increase ceramide levels in cells and thus induce their apoptosis or death. Based on this earlier observation, the drug had entered clinical trials for treatment of breast cancer. However, the earlier studies investigating fenretinide action had relied on a thin-layer chromatography technique that could not distinguish ceramides from dihydroceramides, the latter, according to dogma, being inert. Merrill found that fenretinide induced sphingolipids derived from the dihydroceramide precursor rather than coming from ceramide. Subsequent studies revealed that it was a potent inhibitor of Des1 (43, 44). Thus, a novel molecular target for the drug was identified, and the search for new mechanisms of fenretinide and/or dihydrosphingolipid action ensued.

As ceramides had been shown to antagonize insulin action, and fenretinide had been shown to improve insulin sensitivity and hepatic steatosis *in vivo* (22, 23), attention quickly turned toward the idea that inhibition of the desaturase might prove useful for treating metabolic disease. Indeed, knockdown of Des1 in cultured myotubes prevented the antagonistic effects of saturated fatty acids on insulin signaling (20, 45), and muscles from mice haploinsufficient for Des1 were protected from lipid- and glucocorticoid-induced insulin resistance (16). Moreover, palmitate was shown to induce the enzyme *in vitro* (20, 45), and high-fat feeding did so *in vivo* (20). Lastly, fenretinide inhibited the enzyme *in vivo* in both wild-type and high-fat-fed mice, as detected by alterations in ceramide/dihydroceramide ratios, and this accounted at least partially for the drug insulin sensitizing effects (20).

Dihydroceramides, autophagy, and steatosis. When Merrill's group discovered that fenretinide inhibited Des1, they also found that both it and dihydrosphingolipids induced autophagy (43). Subsequent studies demonstrated that other Des1 inhibitors recapitulated this effect (36, 46, 47). This is particularly interesting to those of us studying metabolic diseases, as autophagy is a proposed mechanism for clearing excess lipid in the liver and thus

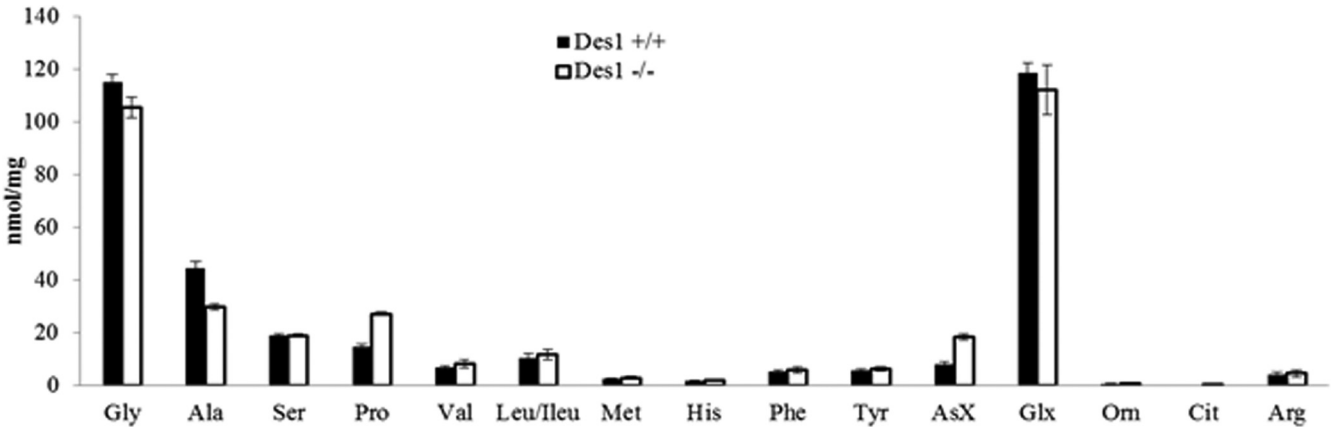

FIG 15 Des1 ablation does not markedly alter amino acid levels. Amino acid levels were quantified in $Des1^{+/+}$ and $Des1^{-/-}$ cells by mass spectroscopy (done by the Stedman Center at Duke University).

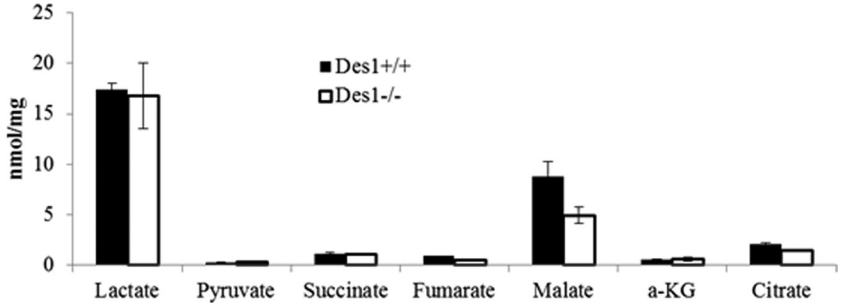

FIG 16 Des1 ablation does not markedly alter the levels of various citric acid cycle intermediates. Organic acid profiles in the knockout and wild-type cells were quantified by mass spectroscopy by the Stedman Center at Duke University.

could serve as a means of ameliorating hepatic steatosis, nonalcoholic steatohepatitis (NASH), and nonalcoholic fatty liver disease (NAFLD) (48–50). Herein, we tested the role of Des1 in autophagy using genetic ablation of the gene rather than relying on pharmacological inhibitors. This method negates concerns related to nonspecific pharmacological effects or incomplete inhibition of the enzyme. As shown herein, Des1 ablation potently induced autophagy, as determined by a number of different molecular readouts (i.e., visualization of the autophagosome by fluorescent or electron microscopy, detection of the active form of LC3, quantification of Atg proteins, etc.).

A major accomplishment of this study was the elucidation of a mechanism by which Des1 inhibition triggers this starvation pathway. Specifically, cells lacking Des1 demonstrated impaired ATP synthesis, likely because of the reduction of complex IV of the electron transport chain. The resulting decrease in ATP leads to activation of Ampk and the induction of the autophagic response. Treatment with ATP and/or knockdown of Ampk prevented the autophagy, confirming their role in the autophagy associated with Des1 ablation. Interestingly, a similar mechanism accounts for the actions of metformin. Metformin inhibits complex I of the electron transport chain, leading to a similar impairment in ATP synthesis and activation of Ampk (5, 51, 52).

An enigma that remains is how Des1 inhibition reduces complex IV levels. While it could be that the Des1 protein has stabilizing properties, an alternative possibility is that the lipid products themselves are important for complex IV assembly or stability. Indeed, inhibition of production of all sphingolipids with myriocin or fumonisin B1 restored initial ATP synthesis rates, suggesting that the lipids were responsible for the impairment in mitochondrial function. We note, however, that in most assays the mitochondria appeared normal and functional (e.g., levels of citric acid cycle intermediates, citrate synthase activity, number of mitochondria, membrane potential, etc.). Thus, the change in sphingolipid levels seemed to cause a specific change in ATP synthesis caused by disrupting the electron transport chain. Just prior to the submission of this article, the Zigdon group demonstrated that ablation of a particular ceramide synthase (CerS2) led to a similar decrease in complex IV (53). As in our studies, the ablation of CerS2 led to a reduction in certain ceramide species and an increase in sphinganine, which is consistent with the idea that specific sphingolipids positively or negatively modulate complex IV assembly or stability.

Ceramides, Akt/PKB, and insulin resistance. The effect of Des1 depletion on Akt/PKB activation was anticipated, as we previously demonstrated that ceramide, but not dihydroceramide, inhibited Akt/PKB activation (24, 26). In addition to mediating nutrient handling, Akt activates anabolic pathways (e.g., glycogen and protein synthesis) while inhibiting catabolism, leading to a marked upregulation in nutrient storage. Akt also stimulates prosurvival and inhibits autophagic enzymes, leading to a net increase in cellular growth and stability. Ceramide opposes nearly all of these Akt actions (54). Both exogenous and endogenous ceramides inhibit Akt phosphorylation and activation without blocking any upstream signaling events (26, 55). In skeletal muscle and fat, this diminution in Akt leads to a decrease in cell surface GLUT4 expression and a reduction in the activity of anabolic enzymes. The effects of ceramide can be negated by the overexpression of constitutively active forms of Akt, identifying this molecule as an essential mediator of ceramide effects (26).

Ceramide inhibits Akt action by two separable mechanisms: first, it promotes Akt dephosphorylation via protein phosphatase 2A (PP2A) (56, 57), which is reportedly a direct target of the sphingolipid; second, it prevents Akt translocation via another putative target, PKCζ (58, 59). The relative importance of either pathway varies by cell type and is influenced by the amount of caveolae in the cell, as the PKCξ-dependent pathway requires functional caveolae (60). Interestingly, the Des1$^{-/-}$ cells demonstrate less PP2A activity and a smaller amount of the PP2A catalytic subunit (34).

Conclusions. Inhibition of sphingolipid synthesis has been considered by many pharmaceutical companies as a means for combating insulin resistance and metabolic disease, and compounds targeting serine palmitoyltransferase (SPT), the first enzyme required for ceramide's *de novo* biosynthesis, have been generated. Fewer attempts have been made to develop inhibitors for Des1. Studies presented herein suggest that Des1 inhibitors may introduce a different spectrum of effects than inhibitors of SPT, owing to the dihydrosphingolipids that accumulate and modulate mitochondrial function. As these lipids are normally rare, one could easily monitor drug efficacy by looking for their appearance. The concern of course relates to the unanticipated side effects associated with generating an entirely new spectrum of lipids in the cell. However, the fact that such an inhibitor has made it to phase III clinical trials for cancer gives a modicum of hope that such a strategy could be both safe and efficacious. An important future step will be to determine if the autophagic induction

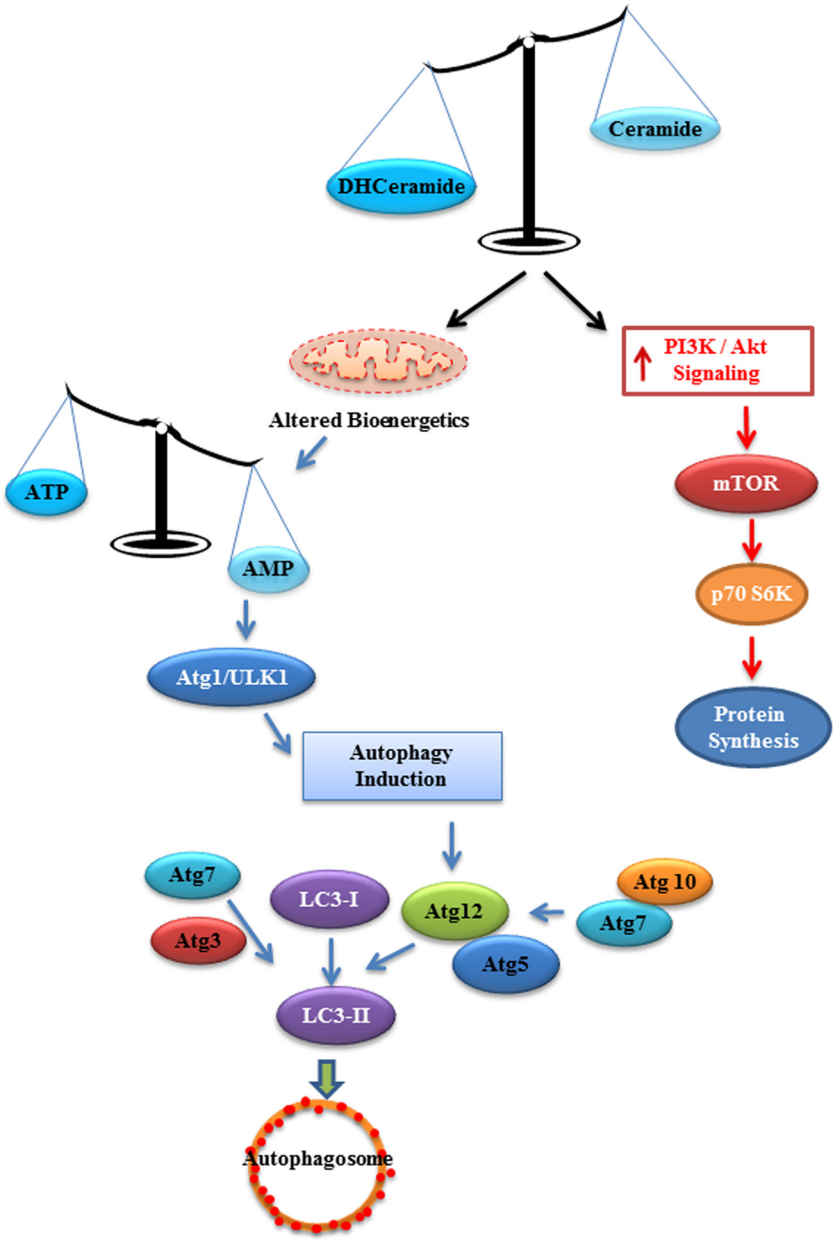

FIG 17 Des1 ablation alters bioenergetics *in vitro*. Proposed schematic depicting how Des1 ablation activates both anabolic and catabolic pathways simultaneously.

accounts for the broad spectrum of metabolic effects associated with Des1 depletion.

ACKNOWLEDGMENTS

This work was supported by the National Medical Research Council (IRG09may004 to S.A.S.); the National Institutes of Health grants R01DK081456-01 (to S.A.S.) and DK58398 to Christopher Newgard; the Singapore Ministry of Education Academic Research Fund MOE2009-T2-2-016 (to S.A.S.); and the Duke-NUS Signature Research Program funded by the Agency for Science, Technology and Research, Singapore, and the Ministry of Health, Singapore (to S.A.S.).

We acknowledge Lexicon Pharmaceuticals, Inc., for the dihydroceramide desaturase (ENZ584T1) knockout mice.

We disclose that there is no conflict of interest.

REFERENCES

1. **Hay N.** 2011. Interplay between FOXO, TOR, and Akt. Biochim. Biophys. Acta **1813**:1965–1970.
2. **Zhang X, Tang N, Hadden TJ, Rishi AK.** 2011. Akt, FoxO and regulation of apoptosis. Biochim. Biophys. Acta **1813**:1978–1986.
3. **Hers I, Vincent EE, Tavare JM.** 2011. Akt signalling in health and disease. Cell. Signal. **23**:1515–1527.
4. **Hardie DG, Ross FA, Hawley SA.** 2012. AMPK: a nutrient and energy sensor that maintains energy homeostasis. Nat. Rev. Mol. Cell Biol. **13**: 251–262.
5. **Hardie DG.** 2011. AMP-activated protein kinase: an energy sensor that regulates all aspects of cell function. Genes Dev. **25**:1895–1908.
6. **Chavez JA, Summers SA.** 2012. A ceramide-centric view of insulin resistance. Cell Metab. **15**:585–594.
7. **Chavez JA, Summers SA.** 2010. Lipid oversupply, selective insulin resis-

tance, and lipotoxicity: molecular mechanisms. Biochim. Biophys. Acta **1801**:252–265.
8. **Jornayvaz FR, Shulman GI.** 2012. Diacylglycerol activation of protein kinase cepsilon and hepatic insulin resistance. Cell Metab. **15**:574–584.
9. **Anonymous.** 2004. PPAR activators and gastroenterology. Drug News Perspect. **17**:683–685.
10. **Zhang QJ, Holland WL, Wilson L, Tanner JM, Kearns D, Cahoon JM, Pettey D, Losee J, Duncan B, Gale D, Kowalski CA, Deeter N, Nichols A, Deesing M, Arrant C, Ruan T, Boehme C, McCamey DR, Rou J, Ambal K, Narra KK, Summers SA, Abel ED, Symons JD.** 2012. Ceramide mediates vascular dysfunction in diet-induced obesity by PP2A-mediated dephosphorylation of the eNOS-Akt complex. Diabetes **61**: 1848–1859.
11. **Shimabukuro M, Higa M, Zhou YT, Wang MY, Newgard CB, Unger RH.** 1998. Lipoapoptosis in beta-cells of obese prediabetic fa/fa rats. Role of serine palmitoyltransferase overexpression. J. Biol. Chem. **273**:32487–32490.
12. **Shimabukuro M, Zhou Levi Y-TM, Unger RH.** 1998. Fatty acid-induced B cell apoptosis: a link between obesity and diabetes. Proc. Nat. Acad. Sci. **95**:2498–2502.
13. **Cariou B, Charbonnel B, Staels B.** 2012. Thiazolidinediones and PPARgamma agonists: time for a reassessment. Trends Endocrinol. Metab. **23**: 205–215.
14. **Papaetis GS, Orphanidou D, Panagiotou TN.** 2011. Thiazolidinediones and type 2 diabetes: from cellular targets to cardiovascular benefit. Curr. Drug Targets **12**:1498–1512.
15. **Hardie DG, Ross FA, Hawley SA.** 2012. AMP-activated protein kinase: a target for drugs both ancient and modern. Chem. Biol. **19**:1222–1236.
16. **Holland WL, Brozinick JT, Wang LP, Hawkins ED, Sargent KM, Liu Y, Narra K, Hoehn KL, Knotts TA, Siesky A, Nelson DH, Karathanasis SK, Fontenot GK, Birnbaum MJ, Summers SA.** 2007. Inhibition of ceramide synthesis ameliorates glucocorticoid-, saturated-fat-, and obesity-induced insulin resistance. Cell Metab. **5**:167–179.
17. **Park TS, Hu Y, Noh HL, Drosatos K, Okajima K, Buchanan J, Tuinei J, Homma S, Jiang XC, Abel ED, Goldberg IJ.** 2008. Ceramide is a cardiotoxin in lipotoxic cardiomyopathy. J. Lipid Res. **49**:2101–2112.
18. **Hojjati MR, Li Z, Zhou H, Tang S, Huan C, Ooi E, Lu S, Jiang XC.** 2005. Effect of myriocin on plasma sphingolipid metabolism and atherosclerosis in *apoE*-deficient mice. J. Biol. Chem. **280**:10284–10289.
19. **Bikman BT, Summers SA.** 2011. Sphingolipids and hepatic steatosis. Adv. Exp. Med. Biol. **721**:87–97.
20. **Bikman BT, Guan Y, Shui G, Siddique MM, Holland WL, Kim JY, Fabrias G, Wenk MR, Summers SA.** 2012. Fenretinide prevents lipid-induced insulin resistance by blocking ceramide biosynthesis. J. Biol. Chem. **287**:17426–17437.
21. **Veterans Medical Research Foundation.** 2011, posting date. A randomized, double-blind study of the effects of fenretinide administered in subjects with obesity. ClinicalTrials.gov. Veterans Medical Research Foundation, San Diego, CA.
22. **Preitner F, Mody N, Graham TE, Peroni OD, Kahn BB.** 2009. Long-term fenretinide treatment prevents high-fat diet-induced obesity, insulin resistance, and hepatic steatosis. Am. J. Physiol. Endocrinol. Metab. **297**: E1420–E1429.
23. **Yang Q, Graham TE, Mody N, Preitner F, Peroni OD, Zabolotny JM, Kotani K, Quadro L, Kahn BB.** 2005. Serum retinol binding protein 4 contributes to insulin resistance in obesity and type 2 diabetes. Nature **436**:356–362.
24. **Summers SA, Garza LA, Zhou H, Birnbaum MJ.** 1998. Regulation of insulin-stimulated glucose transporter GLUT4 translocation and Akt kinase activity by ceramide. Mol. Cell. Biol. **18**:5457–5464.
25. **Verdu J, Buratovich MA, Wilder EL, Birnbaum MJ.** 1999. Cell-autonomous regulation of cell and organ growth in Drosophila by Akt/PKB. Nat. Cell Biol. **1**:500–506.
26. **Zhou H, Summers SA, Birnbaum MJ, Pittman RN.** 1998. Inhibition of Akt kinase by cell-permeable ceramide and its implications for ceramide-induced apoptosis. J. Biol. Chem. **273**:16568–16575.
27. **Datta SR, Brunet A, Greenberg ME.** 1999. Cellular survival: a play in three Akts. Genes Dev. **13**:2905–2927.
28. **Khwaja A.** 1999. Akt is more than just a bad kinase. Nature **401**:33–34.
29. **Yamaguchi H, Wang HG.** 2001. The protein kinase PKB/Akt regulates cell survival and apoptosis by inhibiting Bax conformational change. Oncogene **20**:7779–7786.
30. **Peralta ER, Edinger AL.** 2009. Ceramide-induced starvation triggers homeostatic autophagy. Autophagy **5**:407–409.
31. **Guenther GG, Peralta ER, Rosales KR, Wong SY, Siskind LJ, Edinger AL.** 2008. Ceramide starves cells to death by downregulating nutrient transporter proteins. Proc. Natl. Acad. Sci. U. S. A. **105**:17402–17407.
32. **Pettus BJ, Chalfant CE, Hannun YA.** 2002. Ceramide in apoptosis: an overview and current perspectives. Biochim. Biophys. Acta **1585**:114–125.
33. **Hannun YA, Obeid LM.** 2002. The ceramide-centric universe of lipid-mediated cell regulation: stress encounters of the lipid kind. J. Biol. Chem. **277**:25847–25850.
34. **Siddique MM, Bikman BT, Wang L, Ying L, Reinhardt E, Shui G, Wenk MR, Summers SA.** 2012. Ablation of dihydroceramide desaturase confers resistance to etoposide-induced apoptosis in vitro. PLoS One **7**:e44042. doi:10.1371/journal.pone.0044042.
35. **Jiang Q, Rao X, Kim CY, Freiser H, Zhang Q, Jiang Z, Li G.** 2012. Gamma-tocotrienol induces apoptosis and autophagy in prostate cancer cells by increasing intracellular dihydrosphingosine and dihydroceramide. Int. J. Cancer **130**:685–693.
36. **Signorelli P, Munoz-Olaya JM, Gagliostro V, Casas J, Ghidoni R, Fabrias G.** 2009. Dihydroceramide intracellular increase in response to resveratrol treatment mediates autophagy in gastric cancer cells. Cancer Lett. **282**:238–243.
37. **Kabeya Y, Mizushima N, Ueno T, Yamamoto A, Kirisako T, Noda T, Kominami E, Ohsumi Y, Yoshimori T.** 2000. LC3, a mammalian homologue of yeast Apg8p, is localized in autophagosome membranes after processing. EMBO J. **19**:5720–5728.
38. **Egan DF, Shackelford DB, Mihaylova MM, Gelino S, Kohnz RA, Mair W, Vasquez DS, Joshi A, Gwinn DM, Taylor R, Asara JM, Fitzpatrick J, Dillin A, Viollet B, Kundu M, Hansen M, Shaw RJ.** 2011. Phosphorylation of ULK1 (hATG1) by AMP-activated protein kinase connects energy sensing to mitophagy. Science **331**:456–461.
39. **Kim J, Kundu M, Viollet B, Guan KL.** 2011. AMPK and mTOR regulate autophagy through direct phosphorylation of Ulk1. Nat. Cell Biol. **13**: 132–141.
40. **Coor C, Salmon RF, Quigley R, Marver D, Baum M.** 1991. Role of adenosine triphosphate (ATP) and NaK ATPase in the inhibition of proximal tubule transport with intracellular cystine loading. J. Clin. Invest. **87**:955–961.
41. **Munafo DB, Colombo MI.** 2001. A novel assay to study autophagy: regulation of autophagosome vacuole size by amino acid deprivation. J. Cell Sci. **114**:3619–3629.
42. **Mortimore GE, Schworer CM.** 1977. Induction of autophagy by amino-acid deprivation in perfused rat liver. Nature **270**:174–176.
43. **Zheng W, Kollmeyer J, Symolon H, Momin A, Munter E, Wang E, Kelly S, Allegood JC, Liu Y, Peng Q, Ramaraju H, Sullards MC, Cabot M, Merrill AH, Jr.** 2006. Ceramides and other bioactive sphingolipid backbones in health and disease: lipidomic analysis, metabolism and roles in membrane structure, dynamics, signaling and autophagy. Biochim. Biophys. Acta **1758**:1864–1884.
44. **Rahmaniyan M, Curley RW, Jr, Obeid LM, Hannun YA, Kraveka JM.** 2011. Identification of dihydroceramide desaturase as a direct in vitro target for fenretinide. J. Biol. Chem. **286**:24754–24764.
45. **Hu W, Ross J, Geng T, Brice SE, Cowart LA.** 2011. Differential regulation of dihydroceramide desaturase by palmitate versus monounsaturated fatty acids: implications for insulin resistance. J. Biol. Chem. **286**:16596–16605.
46. **Gagliostro V, Casas J, Caretti A, Abad JL, Tagliavacca L, Ghidoni R, Fabrias G, Signorelli P.** 2012. Dihydroceramide delays cell cycle G1/S transition via activation of ER stress and induction of autophagy. Int. J. Biochem. Cell Biol. **44**:2135–2143.
47. **Fabrias G, Munoz-Olaya J, Cingolani F, Signorelli P, Casas J, Gagliostro V, Ghidoni R.** 2012. Dihydroceramide desaturase and dihydrosphingolipids: debutant players in the sphingolipid arena. Progr. Lipid Res. **51**:82–94.
48. **Liu K, Czaja MJ.** 2013. Regulation of lipid stores and metabolism by lipophagy. Cell Death Differ. **20**:3–11.
49. **Czaja MJ.** 2011. Functions of autophagy in hepatic and pancreatic physiology and disease. Gastroenterology **140**:1895–1908.
50. **Amir M, Czaja MJ.** 2011. Autophagy in nonalcoholic steatohepatitis. Exp. Rev. Gastroenterol. Hepatol. **5**:159–166.
51. **Hardie DG.** 2011. Sensing of energy and nutrients by AMP-activated protein kinase. Am. J. Clin. Nutr. **93**:891S–896S.

52. **Hardie DG.** 2011. Energy sensing by the AMP-activated protein kinase and its effects on muscle metabolism. Proc. Nutr. Soc. **70**:92–99.
53. **Zigdon H, Kogot-Levin A, Park JW, Goldschmidt R, Kelly S, Merrill AH, Jr, Scherz A, Pewzner-Jung Y, Saada A, Futerman AH.** 2013. Ablation of ceramide synthase 2 causes chronic oxidative stress due to disruption of the mitochondrial respiratory chain. J. Biol. Chem. **288**: 4947–4956.
54. **Stoica BA, Movsesyan VA, Lea PM, IV, Faden AI.** 2003. Ceramide-induced neuronal apoptosis is associated with dephosphorylation of Akt, BAD, FKHR, GSK-3beta, and induction of the mitochondrial-dependent intrinsic caspase pathway. Mol. Cell. Neurosci. **22**:365–382.
55. **Chavez JA, Knotts TA, Wang LP, Li G, Dobrowsky RT, Florant GL, Summers SA.** 2003. A role for ceramide, but not diacylglycerol, in the antagonism of insulin signal transduction by saturated fatty acids. J. Biol. Chem. **278**:10297–10303.
56. **Salinas M, Lopez-Valdaliso R, Martin D, Alvarez A, Cuadrado A.** 2000. Inhibition of PKB/Akt1 by C2-ceramide involves activation of ceramide-activated protein phosphatase in PC12 cells. Mol. Cell. Neurosci. **15**:156–169.
57. **Dobrowsky RT, Kamibayashi C, Mumby MC, Hannun YA.** 1993. Ceramide activates heterotrimeric protein phosphatase 2A. J. Biol. Chem. **268**:15523–15530.
58. **Stratford S, DeWald DB, Summers SA.** 2001. Ceramide dissociates 3′-phosphoinositide production from pleckstrin homology domain translocation. Biochem. J. **354**:359–368.
59. **Powell DJ, Hajduch E, Kular G, Hundal HS.** 2003. Ceramide disables 3-phosphoinositide binding to the pleckstrin homology domain of protein kinase B (PKB)/Akt by a PKCzeta-dependent mechanism. Mol. Cell. Biol. **23**:7794–7808.
60. **Hajduch E, Turban S, Le Liepvre X, Le Lay S, Lipina C, Dimopoulos N, Dugail I, Hundal HS.** 2008. Targeting of PKCzeta and PKB to caveolin-enriched microdomains represents a crucial step underpinning the disruption in PKB-directed signalling by ceramide. Biochem. J. **410**:369–379.
61. **Frezza C, Cipolat S, Scorrano L.** 2007. Organelle isolation: functional mitochondria from mouse liver, muscle and cultured fibroblasts. Nat. Protoc. **2**:287–295.